Four-body Coulomb explosion of acetylene in collision with highly charged ions

Yingying Wang,[1] Xiaohua Shi,[1] Jiaqi Zhou,[1] Shenyue Xu,[1,*] Dalong Guo,[2,3] Shuncheng Yan,[2,3] Xiaolong Zhu,[2,3] and Xinwen Ma[2,3,†]

[1]*MOE Key Laboratory for Nonequilibrium Synthesis and Modulation of Condensed Matter, School of Science, Xi'an Jiaotong University, Xi'an 710049, China*

[2]*Institute of Modern Physics, Chinese Academy of Sciences, Lanzhou 730000, China*

[3]*University of Chinese Academy of Sciences, Beijing 100049, China*

(Received 19 December 2019; accepted 30 March 2020; published 22 April 2020)

The dynamics of four-body Coulomb explosion of acetylene in collision with 50 keV/u Ne^{8+} are investigated by detecting all four ionic fragments and the scattered projectile in quintuple coincidence. Six different breakup channels of $C_2H_2^{q+}$ cations with $4 \leqslant q \leqslant 8$ are identified. The kinetic energy (KE) distributions of all ionic fragments as well as the total kinetic energy release (KER) distributions are obtained and compared with the calculation results of the point-charge (PC) approximation model for each channel. For symmetric charge distribution channels, the calculations of PC model, in general, agrees well with the peak positions of the measured KER and KE distributions for all three channels with the largest deviation appearing in the breakup of $C_2H_2^{4+}$. However, for asymmetric charge distribution channels, although the KER values calculated by the PC model for the breakup of $C_2H_2^{5+}$ and $C_2H_2^{7+}$ fit very well with experiment, the KEs of the two protons and the two C cations exhibit noticeable discrepancy between experiment and PC model. In addition, it is found that the fragmentation of $C_2H_2^{6+}$ which may lead to either two C^{2+} cations or one C^+ and one C^{3+} cation shows a strong preference for symmetric charge distribution between the two C cations.

DOI: 10.1103/PhysRevA.101.042706

I. INTRODUCTION

The ionization and fragmentation of molecules plays an important role in many fundamental areas, such as radiation damage of biological tissues [1,2], plasmas physics [3], and chemistry of planetary atmosphere and interstellar mediums [4,5]. Once several electrons are removed from a molecule, the multicharged molecular cation is formed and is generally unstable. It intends to dissociate to ionic fragments through the Coulomb explosion (CE) process due to the strong mutual repulsion between different nuclei. The highly charged ion beam is an efficient tool to produce multicharged molecular cations due to its strong electronic field properties. Taking advantage of the fast development in imaging techniques, multicoincidence measurement of all the ionic fragments from the CE of a polyatomic molecule has been achieved [6]. The kinematically complete information obtained from experiment makes it possible to visualize the fragmentation dynamics in detail [7,8] and reconstruct the structure of molecules [6,9].

The point-charge (PC) approximation is a very simple model which is widely used to describe CE process. Under this approximation, the ionic fragments are treated as point charged particles, and the mass and charge of each particle are located at the center of the nuclei. Meanwhile the distances between these points are defined as the equilibrium internuclear distances of the neutral molecule. The motion of each fragment is governed by the Coulomb repulsion from the others. In such a treatment, definite electronic structures of the parent cation and the fragments in the final state are neglected. Strictly speaking, the PC assumption could only be satisfied for bare nuclei such as proton. Nevertheless, the CE of noble gas dimers could be very well described by the PC model since the distance between the center of the two atoms is much longer than the diameter of the atomic cations [10,11].

The CE dynamics of the covalent molecules are much more complicated than the noble gas dimers since the valence electronic orbitals of the covalent molecules are delocalized over the whole molecule. Many existing references have been performed to investigate the CE of molecules and examine the validity of PC model. Among various molecules, the diatomic molecules N_2 [12–17] and CO [17–24] have been frequently investigated. These studies cover a broad range of the charge states of the precursor cations from 2+ up to 10+. It is found that although the PC approximation is a very simple model, the calculated kinetic energy release (KER, defined as the total kinetic energy of all final fragments) in general fit well with the peak values of the measured KER distributions. Nevertheless, obvious discrepancy appears for the widths of the KER distributions [14–16,20,21,24]. For CE of triatomic molecules like CO_2 [9,25] and N_2O [26], the PC model approximately predicts the peak values of the KER distributions, with a systematic trend that the predicted values of PC model are a litter higher than the measured peak positions.

In this paper, we report the investigation of four-body CE of the tetratomic molecule acetylene (C_2H_2) by Ne^{8+} impact. A wealth of published literatures have investigated

*xushenyue@xjtu.edu.cn
†x.ma@impcas.ac.cn

the fragmentation of charged acetylene [8,24,27–45]. Among these studies, the hydrogen migration is a hot topic and has been found to widely exist in the fragmentation of single and double charged acetylene cations [33–45]. As the charge state increases to 3+ or higher, the probability of proton migration becomes extremely low due to the repulsive potential energy surfaces of the multicharged acetylene cations, and the fragmentation is dominated by CE. Besides, the four-body CE of highly charged acetylene has also been extensively investigated with intense laser fields [27–31]. These experiments exhibit an obvious deviation from the PC model that the measured kinetic energy (KE) of the emitted proton is considerably lower than the CE energy calculated at the equilibrium internuclear distances of the neutral molecules. Such a deviation is attributed to the stretching of the CH bonds induced by the laser field [27–29] since the pulse duration is on the order of the time scale of CH bond vibration (∼10 fs).

The projectile energy is chosen as 50-keV/u in the present study corresponding to the interaction timescale of less than 1 fs which is much shorter than molecular vibration period. Consequently, the structure deformation which has been observed in the fragmentation of acetylene induced by femtosecond laser field is eliminated in this fragmentation process. With the present projectile energy the ionization occurs mainly in the outer orbitals of the target [46]. The highly charged feature of the projectile makes it easy to remove several electrons from the target and produce multiply charged $C_2H_2^{q+}$ cations with a very limited degree of excitation [11]. Among various fragmentation channels we focus on the four-body fragmentation of $C_2H_2{}^{q+}$ with $4 \leqslant q \leqslant 8$. Quintuple coincidence measurement of all four ionic fragments in together with the scattered projectile is achieved by employing the reaction microscope [47,48]. The two protons produced in this process are strict point charged particles since there is no electronic structure. In addition, the two protons react sensitively to the potential of the C_2 (or C) cations, and take the majority of the KER due to the small mass compared to C nuclei. These features make acetylene an ideal prototype to study the dynamics of the CE for polyatomic molecules. The measured KE and KER distributions for different four-body CE channels are compared with PC model and discussed in detail.

II. METHODS

A. Experimental details

The experiment was performed using the reaction microscope (also called cold target recoil ion momentum spectroscopy) [47,48] mounted on the 320 kV platform for multidisciplinary research with highly charged ions locating at the Institute of Modern Physics, Chinese Academy of Sciences. Since details of the experimental apparatus could be found in Ref. [49], only a brief account of the experimental method is given here. The well collimated Ne^{8+} beam with the energy of 50-keV/u intersects with acetylene jet produced by diffusing the pure acetylene gas at stagnation pressure of 1.0 bar through a nozzle with diameter of 30 μm. After collision, the ionic fragments generated via CE of the multiionized target molecules are extracted by the homogeneous electric field and

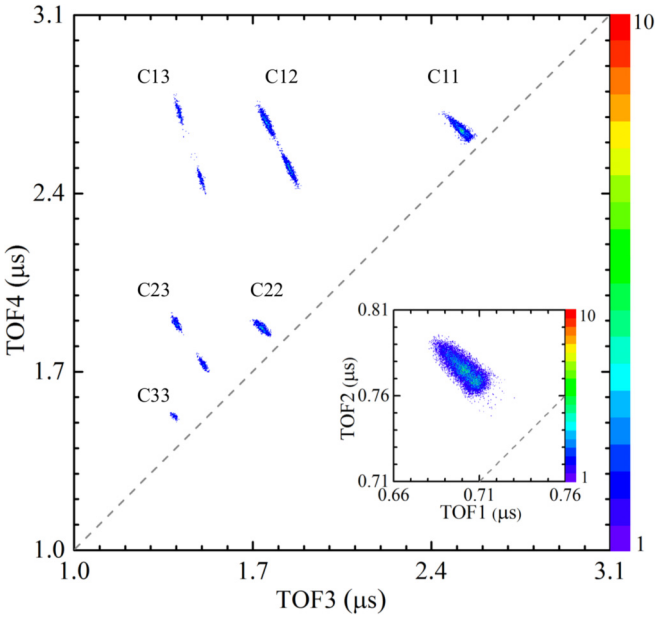

FIG. 1. Four-body CE events displayed in the TOF correlation spectra. Insert displays correlation between the two protons (first and second hits) while the main plot displays correlation between the two C cations (third and fourth hits).

detected by the time-and position-sensitive recoil ion detector. At the same time, an electrostatic deflector downstream of the collision center analyzes and separates the projectiles according to their charge states. The scattered projectiles with charge states of 7+ and 6+ are detected by another time-and position-sensitive detector and recorded in coincidence with the information of the ionic fragments obtained from the recoil ion detector. The time-of-flight (TOF) and the position information of all particles are stored with the event-by-event mode for off-line analysis.

Among various dissociation channels we focus on the four-body fragmentation of $C_2H_2{}^{q+}$ ($4 \leqslant q \leqslant 8$) leading to the products of two protons and two C cations in this study. The precursor $C_2H_2{}^{q+}$ cations are produced through the following two reactions since only Ne^{7+} and Ne^{6+} of the scattered projectiles are recorded in our measurement.

$$Ne^{8+} + C_2H_2 \rightarrow Ne^{7+} + C_2H_2{}^{q+} + (q-1)e^-, \quad (1)$$

$$Ne^{8+} + C_2H_2 \rightarrow Ne^{6+} + C_2H_2{}^{q+} + (q-2)e^-. \quad (2)$$

After ionization, all three chemical bonds including two C–H single bonds and one C ≡ C triple bond break. The species of the ionic fragments are identified according to the TOF information, and consequently the definite fragmentation channels are determined. Figure 1 presents TOF correlation spectra for the four-body CE events with two protons and two C cations completely detected. As displayed in this figure, up to six four-body fragmentation channels are clearly identified according to the TOF of the two C cations. For simplicity, we denote these four-body dissociation channels as C*mn* in the following part of this paper. Here, m and n are charge states of the two C cations, $m + n + 2 = q$, and $m \leqslant n$. These channels are sorted into two groups according to the charge

distribution among the two C cations, the symmetric charge distribution channels C*mm* with $m = n$ and the asymmetric charge distribution channels C*mn* with $m < n$.

(I) symmetric charge distribution channels:

$$\text{C11:}\quad C_2H_2{}^{4+} \rightarrow H^+ + C^+ + C^+ + H^+, \tag{3}$$

$$\text{C22:}\quad C_2H_2{}^{6+} \rightarrow H^+ + C^{2+} + C^{2+} + H^+, \tag{4}$$

$$\text{C33:}\quad C_2H_2{}^{8+} \rightarrow H^+ + C^{3+} + C^{3+} + H^+; \tag{5}$$

(II) asymmetric charge distribution channels:

$$\text{C12:}\quad C_2H_2{}^{5+} \rightarrow H^+ + C^+ + C^{2+} + H^+, \tag{6}$$

$$\text{C13:}\quad C_2H_2{}^{6+} \rightarrow H^+ + C^+ + C^{3+} + H^+, \tag{7}$$

$$\text{C23:}\quad C_2H_2{}^{7+} \rightarrow H^+ + C^{2+} + C^{3+} + H^+. \tag{8}$$

The initial momentum vector of each fragment is reconstructed with the recorded TOF and position information. Consequently, the kinetic energy (KE) of each ionic fragment as well as the kinetic energy release (KER) which is defined as the sum KE of all four ionic fragments is obtained.

B. Point-charge approximation model

In the PC approximation model, the H and C cations are assumed to be point particles with mass and charge. The coordinate as well as KE evolution of each ionic fragment as the function of propagation time is obtained by solving the motion equations of the four separated particles. Details of the calculation are contained in the Appendix. The C ≡ C and C–H bond lengths which are defined as the equilibrium internecular distances between these particles are taken as 0.120 nm and 0.107 nm according to Ref. [50].

As an example we present in Fig. 2 the KE evolution of fragments as a function of propagation time for channel C13. The KEs of the two protons and the two C cations in the final state of the fragmentation are determined to be 51.2, 34.5, 15.4, and 18.5 eV, respectively. Neglecting the possible deviation from real fragmentation dynamics, Fig. 2 presents some typical motion features of the protons and C cations during the four-body CE process. The two protons take most of the KER (around 72%) due to the small mass compared to C atoms. The proton sitting at the C^{3+} side (denoted as $H^+@C^{3+}$) obtains higher KE than the other ($H^+@C^+$) since it experiences a stronger Coulomb repulsion from the nearby C^{3+} cation. Besides, Fig. 2 exhibits clearly that the proton emits much faster than C cation. For example, the two protons obtain 70% of their final KE within 5.3 fs, whereas the KE of C cations only reach 19% at this time.

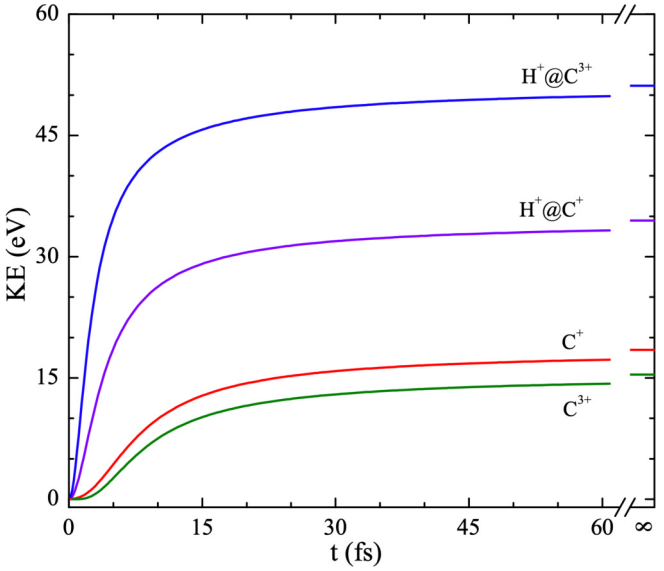

FIG. 2. KE evolution of the two protons and the C cations from C13 breakup channel as a function of propagation time. Solid horizontal lines on the very right of the plot represent KEs of the infinitely separated ionic fragments.

The KE values of each fragment calculated by PC approximation in different channels are listed in Table I accompanying with the peak values of the measured KE distribution curves. In addition, we show in Fig. 5 the ratio between calculated KE (KER) value and the peak position of measured KE (KER) distribution for all six channels to analyze the agreement between PC approximation and the experimental data.

III. RESULTS AND DISCUSSION

KE and KER distributions for symmetric and asymmetric charge distribution channels are presented in Figs. 3 and 4,

TABLE I. KE values of all the ionic fragments as well as KER values of all four-body fragmentation channels. Experimental values are peak positions of the KE (KER) distributions determined by a polynomial fitting procedure. Theoretical values are calculated under the PC approximation model.

	KE of proton (eV)				KE of C cation (eV)				KER (eV)	
Channel	EXP		PC		EXP		PC		EXP	PC
C11	20.0		22.3		4.6		5.7		51.0	56.0
C22	42.6		43.9		19.9		21.9		125.2	131.6
C33	63.4		67.0		45.6		48.5		221.0	231.0
	$@C^{m+}$	$@C^{n+}$	$@C^{m+}$	$@C^{n+}$	C^{m+}	C^{n+}	C^{m+}	C^{n+}		
C12	30.9	31.6	28.5	36.8	10.9	10.8	11.9	10.5	86.4	87.7
C13	41.8	46.5	34.5	51.2	20.1	19.3	18.5	15.4	128.4	119.6
C23	51.9	55.4	50.5	59.4	33.6	33.0	33.7	31.7	173.1	175.3

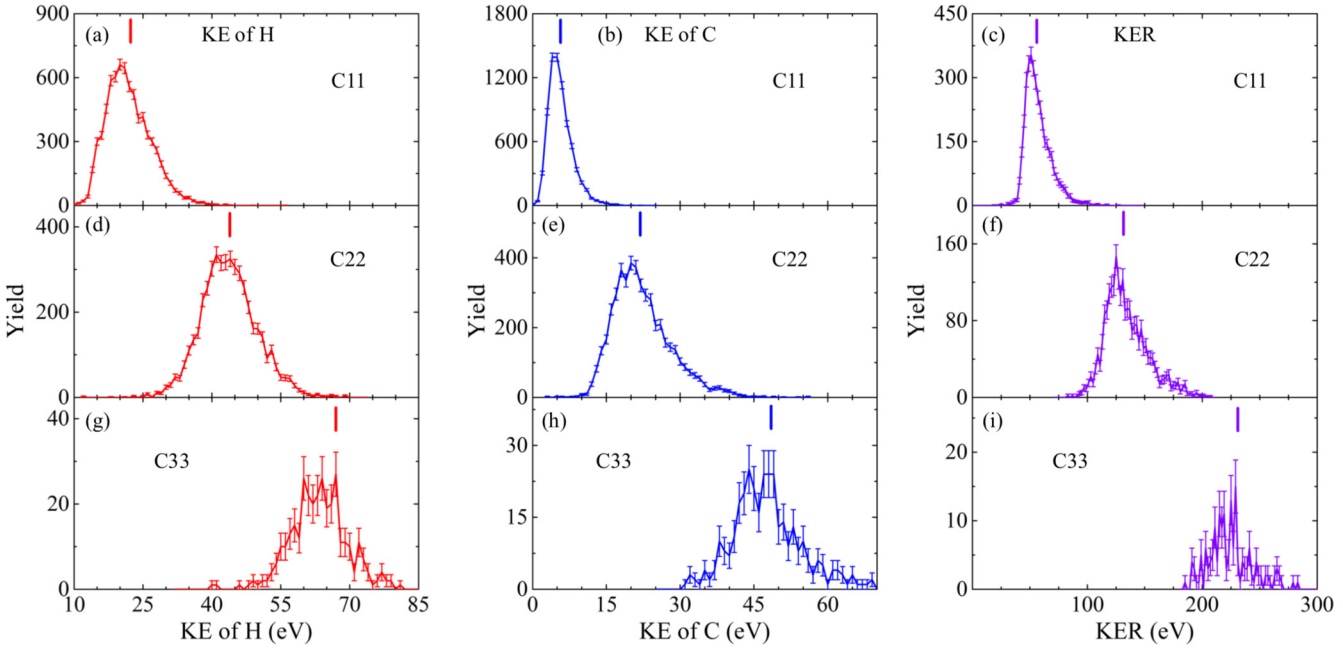

FIG. 3. KE distributions of protons [(a), (d) and (g)], C cations [(b), (e), and (h)], and KER distributions [(c), (f), and (i)] for the symmetric charge distribution channels. Experimental data are shown by the solid lines. Error bars of the data are calculated as square root of the experimental count number. Short vertical bars represent the calculation results of the PC approximation model.

respectively. The peak values of these KE and KER distributions are listed in Table I. As can be seen in Figs. 3 and 4, some of the KE and KER distributions are limited by statistics leading to the indeterminacy of the peak position. A polynomial fitting procedure is applied to the experimental data, and the peak value listed in Table I is taken as the maximum of each fitting curve.

We start our discussion with the symmetric charge distribution channels C11, C22, and C33. As can be seen in Fig. 3, the KER values predicted by the PC model in general fit well with the peak positions of the KER spectra for all three symmetric charge distribution channels with the biggest deviation of around 10% appearing in C11 channel. It is clearly shown in Fig. 5 that the deviation between PC model

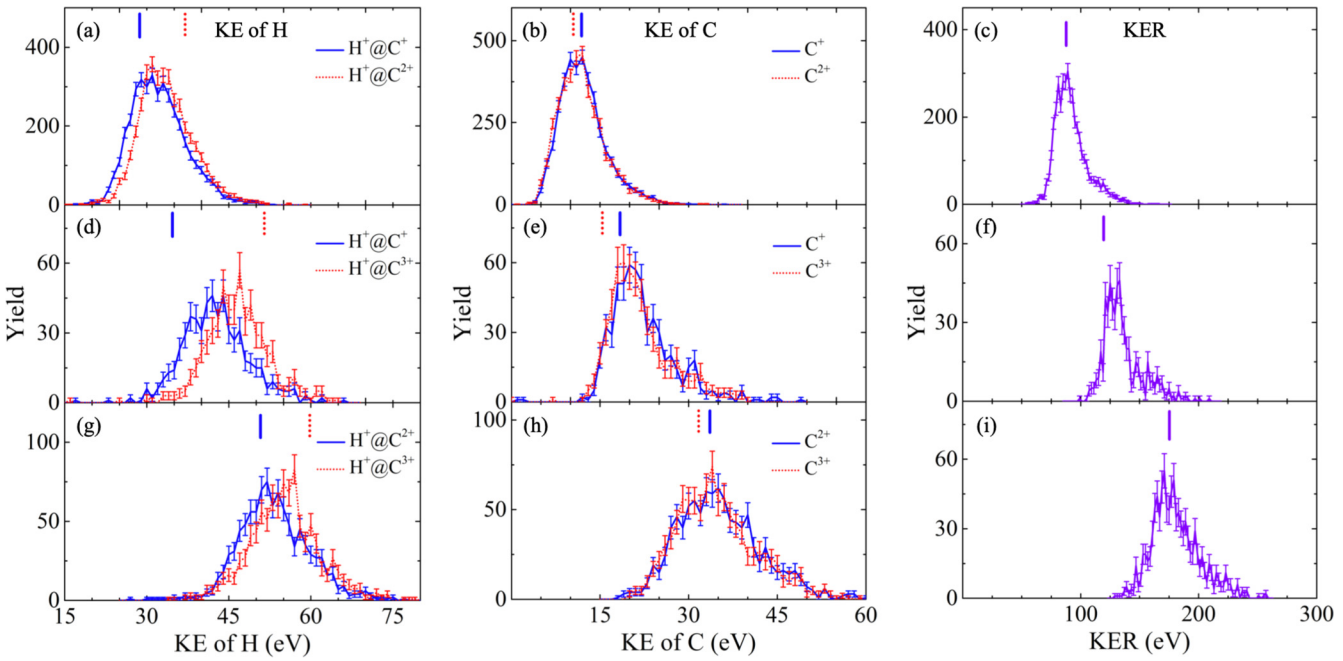

FIG. 4. KE distributions of protons [(a), (d), and (g)], C cations [(b), (e), and (h)], and KER distributions [(c), (f), and (i)] for the asymmetric charge distribution channels. Experimental data are shown by the solid and dotted lines with error bars. Short vertical bars represent the calculation results of the PC approximation model.

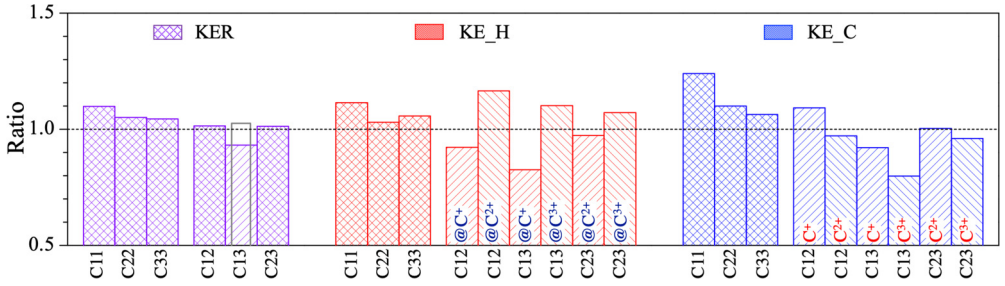

FIG. 5. The ratio between calculated KER (KE) values with PC approximation and the peak positions of the measured KER (KE) distributions for different fragmentation channels. The gray solid rectangle for C13 presents the ratio between calculated KER for C22 with PC approximation and the peak position of the measured KER for C13.

and experiment decreases as the charge state of C^{m+} increases. It could also be seen in Fig. 5 that the agreement between PC calculation and measurement for KE of protons and C^{m+} cations exhibits similar behavior as KER. The biggest deviation appears for channel C11, and such deviation decreases for channels C22 and C33. Such a behavior reveals that the PC approximation is more efficient for fragmentation of the precursor $C_2H_2^{q+}$ cations with higher charge states which is consistent with the CE of multicharged diatomic molecules N_2 [12] and CO [21]. The largest deviation between experiment and the PC approximation observed in C11 with lower charge state indicates that the electronic structures may play reasonable influence to the fragmentation process. Especially for the KE of C^+ cation, the discrepancy of around 24% suggests that the electronic structure of C_2^{2+} precursor ion has a non-neglectable influence on the KEs of the final state fragments.

We now turn to the asymmetric charge distribution channels. Figure 4 presents the KE and KER distributions for asymmetric charge distribution channels C12, C13, and C23. As can be seen in Figs. 4(c) and 4(i) and Fig. 5 that the values calculated by PC model agrees very well with peak positions of the measured KER distributions of C12 and C23 channels. The deviation between PC model and experiment is less than 2% for these two channels, while for channel C13 the agreement between PC model and experiment is relatively poor. Besides, for all the other five channels except C13, the PC model predicts higher KER values than experiment. Contrary to this, the PC model predicts a KER value of 119.6 eV for C13 channel which is about 7% lower than the peak position of the measured KER distribution (128.4 eV). Interestingly, the peak position of KER distribution for C13 is very close to both the calculated and the measured KER values for C22 channel. This is clearly shown by the gray solid rectangle in Fig. 5, which presents the ratio between PC calculation for C22 and the experimental data for C13. The similar behavior was also observed in the CE of diatomic N_2 molecule [15]. A possible explanation of the similarity between KER values of C13 and C22 is the crossing between potential energy surfaces corresponding to the C13 and C22 channels as suggested in Refs. [15,20] for N_2 and CO, respectively.

Figures 4(a), 4(d) and 4(g) present the KE distributions of the protons for the asymmetric charge distribution channels. The PC approximation predicts very different KEs for $H^+@C^{m+}$ and $H^+@C^{n+}$. And the KE differences of the two protons predicted by the PC model for C12, C13 and C23 channels are 8.3, 16.7, and 8.9 eV, respectively. Such difference is mainly due to the different Coulomb potentials from C^{m+} and C^{n+} point charges experienced by the two protons. However, the experimental KE differences according to the values listed in Table I are 0.7, 4.7, and 3.5 eV which are much smaller than the PC calculations. Such deviation between PC model and experiment could also be seen in Fig. 5. The ratio for one of the two protons is always lower than 1.0 while the other is always higher. As is well known, the PC model usually works well for the fragmentation of molecular cations with high charge states [12,21]. This is also observed for symmetric charge distribution channels. However, there are obvious discrepancies between PC model and experiment in the KE of protons for all three asymmetric charge distribution channels. Even for the C23 channel where the precursor cation is in the 7+ high charge state, dramatic difference between PC model and experiment still exists.

The discrepancy between PC model and experiment could also be seen in the KE distributions of the C^{m+} and C^{n+} cations shown in Figs. 4(b), 4(e) and 4(h). The PC approximation leads to a higher KE of C^{m+} (solid blue vertical bar) and a lower KE of C^{n+} (dotted red vertical bar). Besides, the differences between KEs of the two carbon cations with PC approximation are 1.4, 3.1, and 2.0 eV for C12, C13, and C23 channels, respectively. Such differences originate from asymmetric Coulombic repulsion between C cations and protons. However, as shown in Figs. 4(b), 4(e) and 4(h), the experimental KE distributions for the two cations almost overlap with each other. And the measured KE differences between the two C cations are 0.1, 0.8, and 0.6 eV for C12, C13, and C23 channels which are much smaller than the results of PC model.

Thus for asymmetric charge distribution channels, deviation between experiment and PC model is observed not only in the KE of protons but also in the KE of C cations. The agreement of the KER values between experiment and PC model observed for C12 and C23 channels is in fact the average effect of the overestimated KEs of $H^+@C^{n+}$ and C^{m+}, and the underestimated KEs of the $H^+@C^{m+}$ and C^{n+}. Since the vibrational and electronic structures of the molecule are not included in the PC assumption, these two features are possible causes of the observed deviation. Especially, the bending vibration leads to a small deviation ($\approx 10^\circ$) of the molecular structure from the linear geometry [25,51,52]. We

checked the influence of the molecular bending by taking the bond angle between CH and CC bonds to be 170° [51,52] and performing the calculations in two-dimensional space. The calculations for both cis- and trans-bending modes exhibit very similar results as the calculation for linear geometry with small deviations less than 0.3% for the KEs of the two protons, and less than 2% for the C^{m+} and C^{n+} cations. See Table II in Appendix for details. In addition, the stretching vibration leads to the dispersion of the KEs around peak position determined by the initial structure of the neutral molecule [15,24]. Thus we believe that the vibrational structure of the target is not the main reason of the observed deviation between experiment and PC model. The obvious discrepancy between PC model and experiment is probably arising from the electronic structure of the precursor $C_2H_2^{q+}$ and the structures of the C^{m+} and C^{n+} cations in the final state, since the two protons are strict PC particles without any electronic structure. A state-to-state approach with detailed quantum structure information may be necessary to describe the fragmentation process accurately.

We finally focus on the $C_2H_2^{6+}$ cation, which can dissociate to give either C22 or C13 channel. The count ratio between C22 and C13 is determined to be 1:0.24, demonstrating the overwhelming preference for the symmetric charge distribution channel C22. This is consistent with the case of diatomic molecules N_2 [13,16] and CO [18,22,23]. In these studies, the symmetric charge distribution channels are also observed to be the dominant fragmentation pathways for N_2^{4+}, N_2^{6+}, CO^{4+}, and CO^{6+}. In contrast to the covalent molecules listed above, the asymmetric charge distribution channel is observed to be dominant during the fragmentation of van der Waals bounded molecule Ar_2^{4+} [11]. The present results in together with the observation for N_2 and CO may indicate that symmetric charge sharing is the dominant contribution during the breakage of covalent bound.

IV. SUMMARY AND OUTLOOK

The four-body breakup dynamics of $C_2H_2^{q+}$ with $4 \leqslant q \leqslant 8$ are investigated by Ne^{8+} impact. Using the reaction microscope technique, quintuple coincidence measurement of all four ionic fragments and the scattered projectile is achieved for six different four-body breakup channels. The KE distributions of all fragments as well as the total KER distributions for these channels are obtained and compared with the values calculated by PC model.

For the charge symmetric breakup channels, it is found that the peak positions of the measured KER distributions are in general well reproduced by the PC model. The largest deviation around 10% occurs for channel C11, and the deviation decreases significantly for C22 and C33 channels as the charge state of the $C_2H_2^{q+}$ increases. Similar as the KER, the peak positions of the KE distributions of the protons and C cations for charge symmetric breakup channels in general agree well with the calculations of PC model, and the largest deviation appears in C11 channel. However, dramatic discrepancy between experiment and PC model appears for KEs of fragments from asymmetric breakup channels. The PC model predicts obvious different values between the KEs of protons close to C^{m+} and C^{n+} due to the different Coulomb repulsion experienced by the two protons, while such difference is observed to be much smaller in the measurement. The PC model also overestimates the KE difference between C^{m+} and C^{n+}. In spite of the discrepancy for KEs of protons and C cations, the calculated KER values fit well with experiment for C12 and C23 channels. The dramatic discrepancy between PC model and experiment for asymmetric breakup channels indicates that the C^{m+} and C^{n+} cations could not be treated as two localized charges. Specific electronic structures of the precursor $C_2H_2^{q+}$ and the C^{m+} and C^{n+} products should be considered to describe the fragmentation process accurately. In addition, we found that the fragmentation of $C_2H_2^{6+}$ which could lead to either C22 or C13 channel shows a strong preference for the symmetric charge distribution channel.

ACKNOWLEDGMENTS

The work was joint supported by the National Key Research and Development Program of China under Grant No. 2017YFA0402300, the National Natural Science Foundation of China under Grant Nos. U1432122 and 11674332, the China Post-doctoral Science Foundation under Grant No. 2017M613100. The authors acknowledge the 320-kV platform staff at Institute of Modern Physics, Chinese Academy of Sciences for their technical support. SX is indebted to Ran Li for his support in numerical calculations.

APPENDIX: COMPUTATIONAL DETAILS

1. Calculation in one-dimensional space

In the PC approximation model, the motions of all four particles after fragmentation are driven by Coulomb repulsion between each other. These motions propagate in one dimension (x coordinate) due to the linear configuration of the acetylene molecule [Fig. 6(a)]. The equation of motion is written as

$$F_i = m_i x_i''(t), \tag{A1}$$

where $i = 1, \ldots, 4$ indicate the four particles and m_i is the mass of each particle. The resultant force F_i experienced by the particle i from Coulomb repulsion of the other three

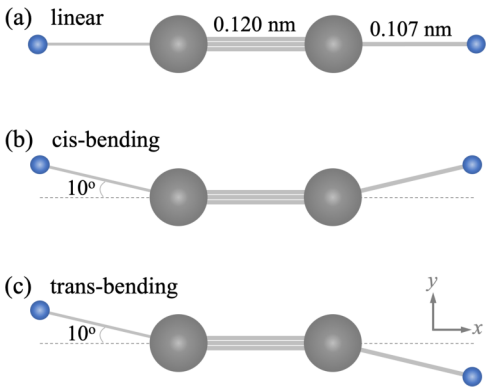

FIG. 6. Structure of the (a) linear, (b) cis-bending, and (c) trans-bending acetylene.

TABLE II. Comparison of calculated KEs (in eV) between linear, cis- and trans-bending structures shown in Fig. 6(a), 6(b), and 6(c) for the asymmetric charge distribution channels.

	$H@C^{m+}$			$H@C^{n+}$			C^{m+}			C^{n+}		
Channel	linear	cis	trans	linear	cis	trans	linear	cis	trans	linear	cis	trans
C12	28.492	28.490	28.508	36.735	36.697	36.701	11.943	11.932	11.940	10.544	10.710	10.652
C13	34.467	34.459	34.498	51.168	51.076	51.093	18.462	18.398	18.423	15.418	15.721	15.612
C23	50.512	50.416	50.436	59.418	59.264	59.281	33.684	33.789	33.789	31.700	32.009	31.944

particles is written as

$$F_i = k \sum_{j \neq i} \frac{q_i\, q_j}{(x_i(t) - x_j(t))^2}. \tag{A2}$$

Here, k is the Coulomb constant, j denotes the other three particles except i, while q_i and q_j are charges of the particles i and j. The initial conditions of the CE are four point particles at rest, i.e.,

$$x_i'(0) = 0. \tag{A3}$$

The two protons and two C cations are separated with distances between each other defined by the C ≡ C and C–H bond lengths of neutral molecules. The value of bond lengths are taken as 0.120 nm and 0.107 nm for C ≡ C and C–H respectively according to Ref. [50]. After solving the coupled equations of motion numerically the KE of each particle as the function of the propagation time is given by

$$E_i(t) = \tfrac{1}{2}\, m_i\, (x_i'(t))^2. \tag{A4}$$

The KE of the ionic fragment in the final state ($t \to \infty$) is written as

$$E_i = \tfrac{1}{2}\, m_i\, (x_i'(\infty))^2, \tag{A5}$$

while the KER is defined as the total KE of all four ionic fragments

$$KER = \sum_i E_i. \tag{A6}$$

2. Calculation in two-dimensional space

The most probable bond angle between CH and CC bonds is smaller than 180° due to bending vibration of the molecule [25,51,52]. This causes a small deviation (≈10°) of the molecular structure from the linear geometry [51,52]. Since both cis- and trans-bending leads to a coplanar structure [Figs. 6(b) and 6(c)], the calculation in two-dimensional (x, y) space is necessary.

The equations of motions in two-dimensional space are written as

$$F_i x = m_i\, x_i''(t), \tag{A7}$$

$$F_i y = m_i\, y_i''(t). \tag{A8}$$

Here, $i = 1, \ldots, 4$ indicate the four particles, m_i is the mass of each particle. $F_i x$ and $F_i y$ are the x and y components of the force experienced by the particle i from Coulomb repulsion of the other three particles. They are written as

$$F_i x = k \sum_{j \neq i} \frac{q_i\, q_j\, (x_j(t) - x_i(t))}{[(x_i(t) - x_j(t))^2 + (y_i(t) - y_j(t))^2]^{\frac{3}{2}}}, \tag{A9}$$

$$F_i y = k \sum_{j \neq i} \frac{q_i\, q_j\, (y_j(t) - y_i(t))}{[(x_i(t) - x_j(t))^2 + (y_i(t) - y_j(t))^2]^{\frac{3}{2}}}. \tag{A10}$$

The initial coordinates of the four particles for cis- and trans-bending are defined by the structures shown in Figs. 6(b) and 6(c), respectively. All four particles are at rest at the beginning of the propagation, i.e.,

$$x_i'(0) = 0, \tag{A11}$$

$$y_i'(0) = 0. \tag{A12}$$

The KE of each particle as the function of the propagation time is given by

$$E_i(t) = \tfrac{1}{2}\, m_i\, [(x_i'(t))^2 + (y_i'(t))^2]. \tag{A13}$$

The KE of the ionic fragment in the final state ($t \to \infty$) is written as

$$E_i = \tfrac{1}{2}\, m_i\, [(x_i'(\infty))^2 + (y_i'(\infty))^2]. \tag{A14}$$

Table II presents the calculation results for the asymmetric charge distribution channels with three different structures shown in Fig. 6. The deviations between KEs with cis- and trans-bending and KEs with linear geometry are less than 0.26% for protons and less than 1.97% for C cations.

[1] S. Xu, D. Guo, X. Ma, X. Zhu, W. Feng, S. Yan, D. Zhao, Y. Gao, S. Zhang, X. Ren, Y. Zhao, Z. Xu, A. Dorn, L. S. Cederbaum, and N. V. Kryzhevoi, Angew. Chem. Int. Ed. **57**, 17023 (2018).

[2] X. Ren, E. Wang, A. D. Skitnevskaya, A. B. Trofimov, K. Gokhberg, and A. Dorn, Nat. Phys. **14**, 1062 (2018).

[3] R. K. Janev, *Atomic and Molecular Processes in Fusion Edge Plasmas* (Plenum, New York, 1995).

[4] P. V. Sada, G. L. Bjoraker, D. E. Jennings, G. H. McCabe, and P. N. Romani, Icarus **136**, 192 (1998).

[5] A. G. G. M. Tielens, Rev. Mod. Phys. **85**, 1021 (2013).

[6] M. Pitzer, M. Kunitski, A. S. Johnson, T. Jahnke, H. Sann, F. Sturm, L. P. H. Schmidt, H. Schmidt-Böcking, R. Dörner, J. Stohner, J. Kiedrowski, M. Reggelin, S. Marquardt, A. Schießer, R. Berger, and M. S. Schöffler, Science **341**, 1096 (2013).

[7] N. Neumann, D. Hant, L. P. H. Schmidt, J. Titze, T. Jahnke, A. Czasch, M. S. Schöffler, K. Kreidi, O. Jagutzki, H. Schmidt-Böcking, and R. Dörner, Phys. Rev. Lett. **104**, 103201 (2010).

[8] S. Xu, X. L. Zhu, W. T. Feng, D. L. Guo, Q. Zhao, S. Yan, P. Zhang, D. M. Zhao, Y. Gao, S. F. Zhang, J. Yang, and X. Ma, Phys. Rev. A **97**, 062701 (2018).

[9] E. Wang, X. Shan, Z. Shen, M. Gong, Y. Tang, Y. Pan, K.-C. Lau, and X. Chen, Phys. Rev. A **91**, 052711 (2015).

[10] B. Ulrich, A. Vredenborg, A. Malakzadeh, M. Meckel, K. Cole, M. Smolarski, Z. Chang, T. Jahnke, and R. Dörner, Phys. Rev. A **82**, 013412 (2010).

[11] J. Matsumoto, A. Leredde, X. Flechard, K. Hayakawa, H. Shiromaru, J. Rangama, C. L. Zhou, S. Guillous, D. Hennecart, T. Muranaka, A. Mery, B. Gervais, and A. Cassimi, Phys. Rev. Lett. **105**, 263202 (2010).

[12] C. P. Safvan and D. Mathur, J. Phys. B: At. Mol. Opt. Phys. **27**, 4073 (1994).

[13] A. Remscheid, B. A. Huber, M. Pykavyj, V. Staemmler, and K. Wiesemann, J. Phy. B: At. Mol. Opt. Phys. **29**, 515 (1996).

[14] U. Brinkmann, A. Reinköster, B. Siegmann, U. Werner, H. O. Lutz, and R. Mann, Phys. Scr. T **1999**, 171 (1999).

[15] B. Siegmann, U. Werner, R. Mann, N. M. Kabachnik, and H. O. Lutz, Phys. Rev. A **62**, 022718 (2000).

[16] J. Rajput, S. De, A. Roy, and C. P. Safvan, Phys. Rev. A **74**, 032701 (2006).

[17] D. Mathur, Phys. Rep. **391**, 1 (2004).

[18] K. Wohrer, G. Sampoll, R. L. Watson, M. Chabot, O. Heber, and V. Horvat, Phys. Rev. A **46**, 3929 (1992).

[19] I. Ben-Itzhak, S. G. Ginther, and K. D. Carnes, Phys. Rev. A **47**, 2827 (1993).

[20] I. Ben-Itzhak, S. G. Ginther, V. Krishnamurthi, and K. D. Carnes, Phys. Rev. A **51**, 391 (1995).

[21] L. Adoui, C. Caraby, A. Cassimi, D. Lelièvre, J. P. Grandin, and A. Dubois, J. Phys. B: At. Mol. Opt. Phys. **32**, 631 (1999).

[22] M. Tarisien, L. Adoui, F. Frémont, D. Lelièvre, L. Guillaume, J.-Y. Chesnel, H. Zhang, A. Dubois, D. Mathur, S. Kumar, M. Krishnamurthy, and A. Cassimi, J. Phys. B: At. Mol. Opt. Phys. **33**, L11 (2000).

[23] J. Rajput and C. P. Safvan, Phys. Rev. A **75**, 062709 (2007).

[24] T. Mizuno and A. Itoh, J. Phys: Conf. Ser. **488**, 012027 (2014).

[25] B. Siegmann, U. Werner, H. O. Lutz, and R. Mann, J. Phys. B: At. Mol. Opt. Phys. **35**, 3755 (2002).

[26] A. Khan, L. C. Tribedi, and D. Misra, Phys. Rev. A **96**, 012703 (2017).

[27] C. Cornaggia, D. Normand, and J. Morellec, J. Phys. B: At. Mol. Opt. Phys. **25**, L415 (1992).

[28] X. Xie, S. Roither, M. Schöffler, H. Xu, S. Bubin, E. Lötstedt, S. Erattuphuza, A. Iwasaki, D. Kartashov, K. Varga, G. G. Paulus, A. Baltuška, K. Yamanouchi, and M. Kitzler, Phys. Rev. A **89**, 023429 (2014).

[29] S. Erattupuzha, C. L. Covington, A. Russakoff, E. Lötstedt, S. Larimian, V. Hanus, S. Bubin, M. Koch, S. Gräfe, A. Baltuška, X. Xie, K. Yamanouchi, K. Varga, and M. Kitzler, J. Phys. B: At. Mol. Opt. Phys. **50**, 125601 (2017).

[30] S. Roither, X. Xie, D. Kartashov, L. Zhang, M. Schöffler, H. Xu, A. Iwasaki, T. Okino, K. Yamanouchi, A. Baltuska, and M. Kitzler, Phys. Rev. Lett. **106**, 163001 (2011).

[31] C. Cornaggia, M. Schmidt, and D. Normand, Phys. Rev. A **51**, 1431 (1995).

[32] T. Mizuno, T. Yamada, H. Tsuchida, Y. Nakai, and A. Itoh, J. Phys: Conf. Ser. **163**, 012039 (2009).

[33] A. Alnaser, I. Litvinyuk, T. Osipov, B. Ulrich, A. Landers, E. Wells, C. Maharjan, P. Ranitovic, I. Bochareva, D. Ray, and C. Cocke, J. Phys. B: At. Mol. Opt. Phys. **39**, S485 (2006).

[34] A. Hishikawa, A. Matsuda, M. Fushitani, and E. J. Takahashi, Phys. Rev. Lett. **99**, 258302 (2007).

[35] S. De, J. Rajput, A. Roy, P. N. Ghosh, and C. P. Safvan, Phys. Rev. A **77**, 022708 (2008).

[36] R. Flammini, E. Fainelli, F. Maracci, and L. Avaldi, Phys. Rev. A **77**, 044701 (2008).

[37] M. E.-A. Madjet, Z. Li, and O. Vendrell, J. Chem. Phys. **138**, 094311 (2013).

[38] C. E. Liekhus-Schmaltz, I. Tenney, T. Osipov, A. Sanchez-Gonzalez, N. Berrah, R. Boll, C. Bomme, C. Bostedt, J. D. Bozek, S. Carron, R. Coffee, J. Devin, B. Erk, K. R. Ferguson, R. W. Field, L. Foucar, L. J. Frasinski, J. M. Glownia, M. Gühr, A. Kamalov, J. Krzywinski, H. Li, J. P. Marangos, T. J. Martinez, B. K. McFarland, S. Miyabe, B. Murphy, A. Natan, D. Rolles, A. Rudenko, M. Siano, E. R. Simpson, L. Spector, M. Swiggers, D. Walke, S. Wang, T. Weber, P. H. Bucksbaum, and V. S. Petrovic, Nat. Commun. **6**, 8199 (2015).

[39] C. Burger, N. G. Kling, R. Siemering, A. S. Alnaser, B. Bergues, A. M. Azzeer, R. Moshammer, R. de Vivie-Riedle, M. Kbel, and M. F. Kling, Faraday Discuss. **194**, 495 (2016).

[40] Z. Li, L. Inhester, C. Liekhus-Schmaltz, B. F. E. Curchod, J. W. Snyder, N. Medvedev, J. Cryan, T. Osipov, S. Pabst, O. Vendrell, P. Bucksbaum, and T. J. Martinez, Nat. Commun. **8**, 453 (2017).

[41] Y. H. Jiang, A. Rudenko, O. Herrwerth, L. Foucar, M. Kurka, K. U. Kühnel, M. Lezius, M. F. Kling, J. van Tilborg, A. Belkacem, K. Ueda, S. Düsterer, R. Treusch, C. D. Schröter, R. Moshammer, and J. Ullrich, Phys. Rev. Lett. **105**, 263002 (2010).

[42] X. Gong, Q. Song, Q. Ji, K. Lin, H. Pan, J. Ding, H. Zeng, and J. Wu, Phys. Rev. Lett. **114**, 163001 (2015).

[43] S. Xu, H. Zhao, X. Zhu, D. Guo, W. Feng, K.-C. Lau, and X. Ma, Phys. Chem. Chem. Phys. **20**, 27725 (2018).

[44] Y. Zhang, B. Wang, L. Wei, T. Jiang, W. Yu, R. Hutton, Y. Zou, L. Chen, and B. Wei, J. Chem. Phys. **150**, 204303 (2019).

[45] L. Chen, X. Shan, E. Wang, X. Ren, X. Zhao, W. Huang, and X. Chen, Phys. Rev. A **100**, 062707 (2019).

[46] M. Rødbro, E. Horsdal Pedersen, C. L. Cocke, and J. R. Macdonald, Phys. Rev. A **19**, 1936 (1979).

[47] R. Dörner, V. Mergel, O. Jagutzki, L. Spielberger, J. Ullrich, R. Moshammer, and H. Schmidt-Böcking, Phys. Rep. **330**, 95 (2000).

[48] J. Ullrich, R. Moshammer, A. Dorn, R. Dörner, L. P. H. Schmidt, and H. Schmidt-Böcking, Rep. Prog. Phys. **66**, 1463 (2003).

[49] X. Ma, R. T. Zhang, S. F. Zhang, X. L. Zhu, W. T. Feng, D. L. Guo, B. Li, H. P. Liu, C. Y. Li, J. G. Wang, S. C. Yan, P. J. Zhang, and Q. Wang, Phys. Rev. A **83**, 052707 (2011).

[50] P. J. Linstrom and W. G. Mallard, NIST Chemistry WebBook, National Institute of Standards and Technology, Gaithersburg MD, https://webbook.nist.gov.

[51] W. M. A. Smit and T. V. Dam, J. Mol. Struct. (Theochem) **88**, 273 (1982).

[52] L. Liu and J. T. Muckerman, J. Chem. Phys. **107**, 3402 (1997).